

Longitudinal Behavior Planning with Maneuver Prediction for Urban Driving

Master of Science Thesis

R.P. Willems



Longitudinal Behavior Planning with Maneuver Prediction for Urban Driving

Master of Science Thesis

by

R.P. Willems

to obtain the degree of Master of Science
at the Delft University of Technology,
to be defended publicly on Thursday July 5, 2018 at 12:00.

Student number: 4095979
Project duration: March 1, 2017 – July 5, 2018
Supervisor: Ir. M. Sefati, PEM RWTH Aachen University
Thesis committee: Prof. dr. ir. P. P. Jonker, TU Delft
Dr. J. Alonso-Mora, TU Delft
Dr. ir. R. Happee, TU Delft

An electronic version of this thesis is available at <http://repository.tudelft.nl/>.

Longitudinal Behavior Planning with Maneuver Prediction for Urban Driving

Abstract—One of the remaining challenges in the development of intelligent vehicles is the topic of behavior planning in urban scenarios. Based on perception of the environment around the intelligent vehicle, driving behavior has to be optimized to achieve a comfortable driving experience without sacrificing safety. This work covers the development of a novel longitudinal behavior planning method for an intelligent passenger vehicle in urban scenarios. A multi-layer situation analysis architecture consisting of localization, maneuver prediction and trajectory prediction is used to predict traffic object trajectories on urban intersections and roundabouts. A universal model predictive controller is developed to determine the optimal longitudinal acceleration behavior of the intelligent vehicle online in a variety of urban scenarios, based on the predicted trajectories. Real-time simulations show that the behavior planning method is able to maintain safe driving conditions with reasonable comfort during scenarios with varying traffic maneuvers.

I. INTRODUCTION

According to the World Health Organization (WHO), road traffic accidents are the cause of 1.25 million deaths and many millions of serious injuries per year worldwide [1]. Additionally, traffic accidents result in high economic losses. In 2015, the costs resulting from traffic accidents combined to an estimated €14.2 billion in the Netherlands alone [2]. For approximately 94% of traffic accidents in the U.S.A., driver error is found to be the critical reason leading up to a traffic accident [3]. With the aim to reduce the number of casualties, as well as the economic losses due to traffic accidents, automobile manufacturers and research groups are developing Advanced Driver Assistance Systems (ADAS) that prevent a driver from making errors. Besides the improvement in safety, ADAS have the goal to increase comfort and fuel efficiency in vehicles. From the development of Adaptive Cruise Control (ACC) in the 1990s ([4], [5]), to the implementation of conditionally self driving systems in recent years, such as Tesla's *Autopilot* [6] or Mercedes-Benz' *Intelligent Drive* [7], research focus has been shifting from low level control of the vehicle's actuators to higher level control. Nowadays, one of the remaining challenges in the development of intelligent vehicles is the topic of behavior planning in urban scenarios. This topic, also known as decision making, constitutes the vehicle's ability to optimize driving behavior by combining knowledge of perceived objects and surrounding road users, traffic laws and local road layout, as well as physical limitations and the state of the ego vehicle. Many different approaches have been developed to optimize the acceleration behavior of intelligent vehicles. However, these methods either require prior knowledge of traffic maneuvers, are unable to perform in real-time, have a very narrow action

set, or are incompatible with urban driving. Therefore, in this work, a novel behavior planning method for urban scenarios is developed that is capable of optimized real-time longitudinal control with traffic maneuver prediction.

A. Functional System Architecture

A functional system architecture for intelligent vehicles, shown in Figure 1, is proposed in [8]. It consists of four layers: strategic, tactical, operative and executive. The strategic layer contains the global route planning module which is responsible for general navigation and route planning. The tactical layer consists of the situation analysis and behavior planning module which is responsible for tactical choices about driving behavior such as lane changes and acceleration for merging in traffic. The operative layer contains the trajectory planning and tracking module which finds the optimal path for the vehicle based on the inputs from the higher level control modules. Finally, the executive layer consists of low level control and actuators to follow the path proposed in the operative layer.

This project focuses on the development of a novel behavior planning method for longitudinal control of an intelligent passenger vehicle in urban scenarios. The functional system architecture is relevant for this project because the modular nature of the architecture allows for independent development of the behavior planning module. By using this architecture, the assumption is made that the tasks in the remaining control modules are either solved by other automated systems or by human drivers, leaving the opportunity to focus fully on the development of the behavior planning module.

B. Related Work

One of the earliest implementations of a behavior planning making process in an intelligent vehicle was in the DARPA urban challenge. Competing in this challenge, *Boss*, a vehicle developed by Carnegie Mellon University used a rule-based decision making process to perform driving tasks in an urban environment [9]. This decision process is based on an architecture where a *goal selector* determines in which of the preprogrammed situations the ego vehicle finds itself, followed by the execution of behavior components specific for each situation. The behavior components contain predetermined rules that specify how the vehicle should behave in a given situation. Furthermore, for simple traffic situations these methods have an unparalleled ease of implementation, requiring little more than a few Boolean algebraic equations. However, a practical limitation is that a rule-based decision process is applicable to preprogrammed situations only, making this method of

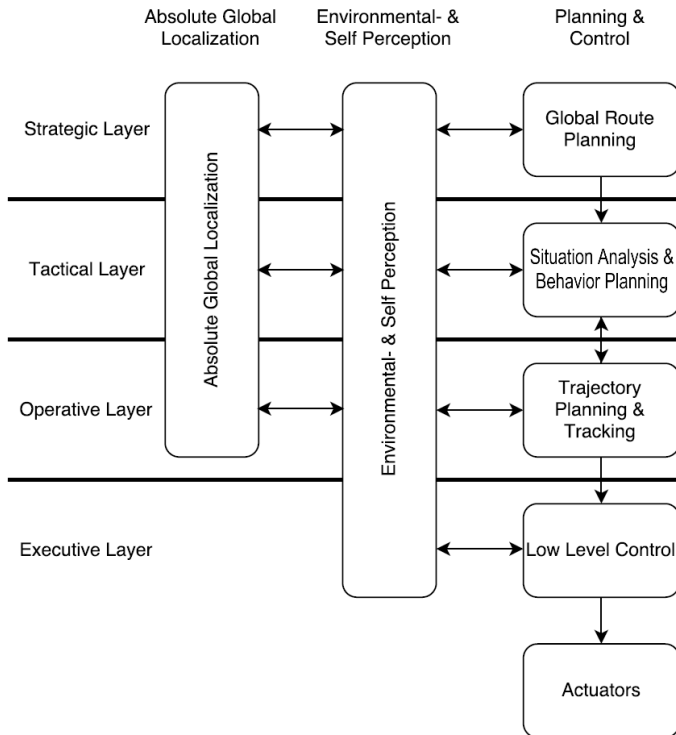


Figure 1: The functional system architecture of an intelligent vehicle consists of four layers: strategic, tactical, reactive operative and executive. Adapted from [8].

behavior planning unsuitable for wide applicability in varying scenarios [10], [11].

A more widely applicable method of behavior planning is the method of Monte-Carlo Tree Search (MCTS) Decision Making. This method, used in [12] for longitudinal and lateral decision making in highway scenarios uses randomly sampled actions to generate a decision tree. The decision tree consists of nodes representing the states of the vehicles, with the initial node representing the current state of the vehicles. From the initial node, a decision tree is generated by sampling a random decision from the available actions, such as accelerating, braking or keeping a constant velocity. The decision leads to the generation of a new node, consisting of the states of the vehicles that follow from the decision. A disadvantage of the Monte-Carlo Tree Search in [12] is that the action set is relatively narrow. The algorithm can only decide between keeping a constant velocity, accelerating or decelerating with a fixed acceleration, stopping or changing lane to the left or the right. Because of this limited action set, it is possible that the optimal driving strategy could not be reached resulting in less desirable maneuvers. Especially in urban scenarios where the ego vehicle is required to merge onto roundabouts and intersections between other vehicles, it is necessary to have wider range of possible acceleration and deceleration values without compromising computational efficiency.

A variation on the tree search method is the Partially Observable Markov Decision Process (POMDP). Just like the MCTS method, this method, used in [13], makes use of decision trees to find the optimal decision set. However, where MCTS evolves the decision tree from a single initial estimated state, the POMDP evolves the decision tree for the entire range of initial state probabilities. For this reason, this method works for partial observability, and thus can find the optimal decision set even when encountered with incomplete or noisy measurements of the states of traffic objects. A disadvantage of this method is that it has very high computational costs. It has been shown in [14] that a POMDP method for urban decision making is able to run in near real-time for an action set of three possible actions. By expanding the action set, the computational costs increase exponentially, making this method impractical for real-time use with a wide action set.

In [11] and [15], a Model Predictive Controller is used for longitudinal and lateral behavior planning in highway scenarios. Model Predictive Control (MPC) based behavior planning utilizes an internal transition model to predict the evolution of states during a finite time horizon. Online optimization of a cost function is used to find the optimal driving behavior. The cost function can be based on vehicle kinematics, road laws, comfort rules and risk indicators, and aims to minimize undesirable actions. The advantage of such a behavior planning method is that it allows for a continuous action space, meaning that the controller is able to optimize the action to an exact acceleration value. In [16], this behavior planning method is extended for use in urban scenarios. It is shown that an MPC based behavior planner is able to provide desirable actions in a variety of simplified urban scenarios. The practical limitation of this work is that it assumes that the path of all traffic objects is known in advance, as well as that these traffic objects maintain a constant velocity.

C. Overview of the Research Project

Based on this literature overview, it can be concluded that there are many different approaches to behavior planning for intelligent vehicles, each with its own benefits and drawbacks. In this project, the focus is on a behavior planning method that follows the criteria:

- Applicable to a variety of urban scenarios
- Capable of real-time performance
- Wide action set to accommodate both comfortable and evasive maneuvers
- Ability to predict traffic maneuvers

Based on these criteria, a Model Predictive Controller-based behavior planning method is the most fitting method for this project. The choice is made to focus fully on longitudinal behavior planning, instead of combining a longitudinal behavior planner with a lane change decision making method. This choice is made because for lane changes, a discrete decision making module is required that is not compatible with this model predictive control based behavior planner. Decisions on lane changes could be included by developing a separate decision process for lateral motion that is run in advance of the longitudinal behavior planning module, such as is done in

[16]. For the development of this behavior planning module the following research questions are posed:

- Can a single model predictive controller be used for behavior planning in a large variety of urban scenarios?
- How can traffic maneuver prediction be implemented in the behavior planning process?
- How will the model predictive controller be able to balance comfort and safety in critical situations?
- Can real-time performance be maintained?

This work covers the development and testing of a model predictive control-based longitudinal behavior planning method with maneuver prediction for use in urban scenarios. Section II describes the methods for developing and evaluating the behavior planning method. In section III, the implementation of the situation analysis and behavior planning module are covered. Section IV shows the evaluation of the behavior planning method through simulations. Lastly, the discussion and conclusion are covered in section V.

II. DEVELOPMENT AND VALIDATION

In order to answer the posed research questions a method of development and validation is determined. The choice is made to simulate the performance of the behavior planning module using IPG Carmaker 5. This real-time virtual test driving software is capable of dynamical simulations of an entire traffic scenario. The convenient architecture of this software allows for specific development of a longitudinal control method of the ego vehicle, without the necessity of manually generating lateral movement trajectories. The simulation software is run through a program developed in C++ that is able to access the simulation data and input the longitudinal control values into the simulation in real-time. The Model Predictive Controller is developed in C++ using the code generation tool within the *Toolkit for Automatic Control and Dynamic Optimization* (ACADO) [17]. This toolkit generates optimized code for non-linear model predictive control, based on the defined control problem functions.

For the development of the behavior planning module, a number of assumptions are made. Firstly, it is assumed that the global localization of the ego-vehicle and traffic objects is handled by an accurate, independent localization method outside of the scope of this work. In the simulations this is handled by reading out the global x and y coordinates for all vehicles directly from the simulation states. Furthermore, traffic priority rules are not applied and traffic objects do not adapt their approach to intersections based on the positioning of the ego-vehicle. This forces the ego-vehicle to yield for traffic objects when necessary, instead of traffic objects yielding for the ego-vehicle. The traffic objects are set up to only adapt their velocity to follow the ego-vehicle after it has passed the intersection or roundabout to prevent rear-end collisions with the ego-vehicle.

A. Evaluation Criteria

The developed controller is evaluated in a selection of scenarios on a roundabout, and an unsignaled four-way intersection and Y-intersection. For each junction, initial conditions

and traffic object maneuvers are varied to show how the behavior planner compensates for changes in the scenario. The performance of the behavior planning module is judged based on the following criteria:

- Safety: Small distances to traffic objects are regarded as less safe.
- Comfort: High values of jerk and acceleration are experienced as uncomfortable.
- Time efficiency: Additional time needed to pass an intersection means the behavior is less time efficient.

The safety criterion is measured as the smallest distance and the lowest *Inter-Vehicle Time* (TIV) between the ego-vehicle and traffic objects. The TIV is calculated as the distance between the centers of the ego-vehicle and traffic object ahead, divided by the longitudinal velocity of the ego-vehicle [18]. As a rule of thumb, the Dutch public prosecutor, as well as many national and international traffic safety organizations recommend an inter-vehicle time of at least 2 seconds [19].

The comfort criterion is measured as the peak longitudinal jerk, and the peak longitudinal acceleration or deceleration of the ego-vehicle. Although no exact acceleration threshold has been found above which longitudinal acceleration is deemed uncomfortable, most studies indicate that longitudinal accelerations and decelerations up to at least 1.5 m s^{-2} are considered acceptable in public transport. Furthermore, Jerk is a strong indicator for comfort, and it has been shown that values of more than 3 m s^{-3} are likely considered unacceptable in public transport [20]. These values for public transport are applicable to intelligent vehicles, because future intelligent vehicles could provide a similar travel experience to public transport, where passengers are not seated in the traditional layout of passenger cars.

Time efficiency is measured as the time it takes for the ego-vehicle to enter an intersection after that intersection is vacated by traffic objects. This criterion will be referred to as the *Time To Intersection* (TTI). A large TTI means that the behavior planning module is conservative and might take more time than desired to complete a driving task, resulting in lower time efficiency. Conversely, a small TTI means that the behavior planning module is assertive and might take more risks to achieve higher time efficiency.

III. SITUATION ANALYSIS AND BEHAVIOR PLANNING

The goal of behavior planning in intelligent vehicles is to predict which vehicle control action will result in the most beneficial driving behavior. To determine which of the possible actions is the most beneficial, a cost function is devised that quantifies the consequences of each action. An optimization algorithm then searches which control action results in the lowest cost.

In this project, a model predictive controller (MPC) is used to find the optimal control actions. The advantage of using an MPC is that this allows for a continuous action space. This means that the controller not only decides whether to accelerate or brake, but rather is able to predict which exact acceleration value would result in the optimal driving behavior. The MPC does this by using a transition model consisting of

differential equations and algebraic equations to predict how a set of initial states and control inputs propagates during a time window. This time window is called the prediction horizon t_H , and consists of a number of samples N_H , referred to as the prediction steps. On each of the prediction steps, the transition model, cost function and constraints are evaluated. An optimization algorithm then determines which combination of control input results in the lowest combined costs during the entire prediction horizon. This optimal control process is repeated at every sampling instance with the new initial states.

A. Situation Analysis

Behavior planning for an intelligent vehicle requires certain knowledge of the surroundings of the vehicle. The behavior planning module needs to be able to predict the future states of the traffic scene, such as the positions and velocities of other vehicles, so that the future consequences of all available actions can be weighed. This part of the behavior planning framework is called situation analysis, and is responsible for predicting the future states of the traffic scene based on the current state of the traffic scene and control inputs. A large variety of state prediction models for traffic can be found in literature. These models can be divided into three categories: physics based motion models, maneuver based motion models, and interaction aware motion models [21]. Physics based motion models, such as the constant velocity model, also known as a single integrator, used in [15] and [16], and the *Intelligent Driver Model* proposed in [22] and used for car following, consist of kinematic or dynamic equations, and are the simplest and most computationally efficient models for predicting the states of traffic objects. Physics based motion models use a set of general models to predict all motion of traffic objects. Because of this general approach, these models are unable to accurately predict specific maneuvers made by traffic objects, and are only accurate when the paths of traffic objects are known a priori, such as in [16].

Maneuver based motion models, such as the Bayesian Network proposed in [23], make use of trained classifiers to predict which of a set of predetermined maneuvers a traffic object will undertake. Based on the maneuver prediction, a maneuver-specific kinematic model is applied that is able to accurately predict the future states of the traffic objects during a small prediction horizon. However, because a model predictive controller uses a fixed internal transition model to predict the future states in the traffic scenario, a specific MPC would need to be formulated for each combination of maneuvers, with a higher-level controller switching between the different MPC controllers. For a scenario with multiple traffic objects, the number of possible maneuver combinations is too large for this solution to be considered practical.

Interaction aware motion models form the most advanced maneuver prediction models [21]. These models consider vehicles to interact and influence each other. These models work by estimating the probability of one vehicle's states based on noisy and incomplete measurements of the current and previous states of all vehicles in a scenario [24]. By using the measurements for all vehicles to predict the motion of a

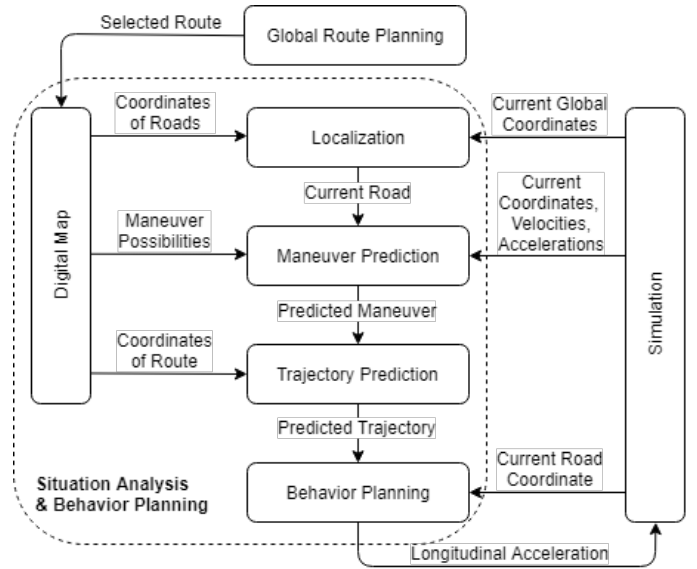


Figure 2: The architecture of behavior planning consists of a digital map, and localization, maneuver prediction, trajectory prediction and behavior planning modules.

single vehicle, the motion model is able to predict interactive behavior between the vehicles. Although these methods can lead to very accurate motion prediction, the computational costs of these methods make them impractical for real-time applications [21].

B. Functional Architecture of Behavior Planning

To achieve the most accurate motion predictions while maintaining a general transition model in the MPC that is capable of behavior planning in a large variety of urban scenarios, the choice is made to take a multi-layered approach to future state prediction. The architecture for this is shown in figure 2.

The architecture of behavior planning consists of a digital map, localization, maneuver prediction, trajectory prediction, and behavior planning modules. Firstly, a digital map is made that includes all road segments and junctions in a particular traffic scene. For each junction, the digital map prescribes which maneuvers are available to the vehicles on each road. These maneuvers are: *Right Turn* (RT), *Straight* (ST) and *Left Turn* (LT). The information in the digital map is used in the localization, maneuver prediction and trajectory prediction modules.

In the localization module, the global coordinates of each vehicle are compared to the available road segments to find on which road segment each traffic object is driving. This information is passed through to a Bayesian network that uses the additional information of velocity, acceleration and position on the road of each traffic object together with the availability of maneuvers to predict which maneuver each traffic object will make. This Bayesian network is developed in [23] specifically for use with IPG Carmaker 5. In this

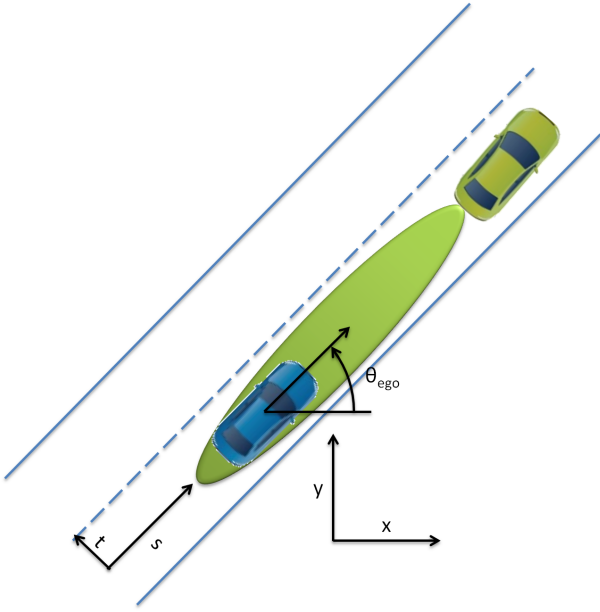


Figure 3: The ellipse around the ego-vehicle indicates the safe zone as defined by the constraints in equation (5). The road coordinate system consists of s , the traveled distance along the lane centerline, and t , the lateral deviation from the lane centerline.

application, the Bayesian networks make use of 10 evidence nodes and 3 binary maneuver nodes to determine which of the available maneuvers is the most likely. For each traffic object, a separate Bayesian network is generated. With the digital map and the knowledge of the current road segment and predicted maneuver, a route prediction can be made for each traffic object. This route prediction is the combination of roads that a traffic object is predicted to take during the prediction horizon. For each traffic object, the road coordinates and global coordinates along the predicted route are sampled from the digital map and stored. Both coordinate systems are shown in figure 3. The road coordinate consists of the s and t coordinates, where the s coordinate follows the lane centerline and indicates the travelled distance of a vehicle. The t coordinate is perpendicular to the lane centerline and represents the lateral deviation from the lane.

A polynomial fitter using ordinary least squares estimation is then used to generate a continuous trajectory in global coordinates as a function of the road coordinate for each vehicle in the scenario. The predicted trajectory of each traffic object comprises a set of two polynomials, shown in equation (1), where x_i and y_i are approximations to the respective global x and y coordinates, and s_i is the longitudinal road coordinate of traffic object i . The coefficients b_{n_i} and c_{n_i} are generated

by the polynomial fitter.

$$\begin{aligned} x_i &= \sum_{n=0}^5 b_{n_i} \cdot s_i^n \\ y_i &= \sum_{n=0}^5 c_{n_i} \cdot s_i^n \end{aligned} \quad (1)$$

For the trajectory prediction of the ego-vehicle, a third polynomial is included that approximates the yaw angle θ_{ego} of the ego-vehicle as a function of the longitudinal road coordinate s_{ego} , with polynomial coefficients $d_{n_{\text{ego}}}$. The resulting set of polynomials for the ego-vehicle is shown in equation (2).

$$\begin{aligned} x_{\text{ego}} &= \sum_{n=0}^5 b_{n_{\text{ego}}} \cdot s_{\text{ego}}^n \\ y_{\text{ego}} &= \sum_{n=0}^5 c_{n_{\text{ego}}} \cdot s_{\text{ego}}^n \\ \theta_{\text{ego}} &= \sum_{n=0}^5 d_{n_{\text{ego}}} \cdot s_{\text{ego}}^n \end{aligned} \quad (2)$$

The reason to use polynomials to represent vehicle trajectories, is that these trajectories can be directly used in the model predictive controller. Because these polynomials consist of a fixed form where the variations in the approximated trajectory only originate from varying the coefficients b_{n_i} , c_{n_i} , $b_{n_{\text{ego}}}$, $c_{n_{\text{ego}}}$ and $d_{n_{\text{ego}}}$ this representation of the trajectory fits with the requirement of the model predictive controller to have a general transition model that is capable of state prediction in a variety of scenarios. The transition model can be adapted to each specific trajectory, simply by feeding the appropriate polynomial coefficients into the MPC. Using polynomials to approximate trajectories does have its disadvantages. Because extrapolation of higher order polynomials tends to lead to highly inaccurate approximations, it is important to predict the trajectory for a longer prediction horizon than is used in the model predictive controller. Furthermore, fitting polynomials of a high order can lead to overfitting to the sampled coordinates, and increases computational costs in the MPC. Therefore the choice is made to use fifth order polynomials to approximate the vehicle trajectories. To validate the accuracy of the fifth order polynomials, three different trajectories are approximated and the resulting global coordinates are compared to the real global coordinates. These trajectories are: driving in a straight line, approaching and entering a roundabout, and approaching an intersection and making a sharp left turn. The median and maximum approximation errors for the three trajectories are shown in Table I. With median approximation errors of 1.8 cm to 5.6 cm the polynomial approximations are sufficiently accurate for this application.

C. Transition Model, Constraints and Cost Function

The polynomial coefficients that approximate the predicted trajectories are used in the transition model of the model predictive controller. The transition model comprises a set

Trajectory	Median error (cm)	Maximum error (cm)
Straight	1.8	5.5
Entering roundabout	5.6	17.1
Left Turn	4.9	20.9

Table I: Median and maximum approximation errors of fifth order polynomial trajectories.

of states, differential equations and algebraic equations to represent the kinematics of the ego vehicle and all traffic objects in a traffic scene. The transition model that is used in this project is a constant acceleration model based on the road coordinate system, with safety constraints based on the global coordinate system. The state X_i of traffic object i is:

$$X_i \in \mathbb{R}^4 = \begin{pmatrix} s_i \\ v_i \\ x_i \\ y_i \end{pmatrix}$$

Where v_i is the longitudinal velocity, x_i is the global x-coordinate, and y_i is the global y-coordinate of traffic object i . The transition model describing the traffic objects is:

$$\begin{aligned} \dot{s}_i &= v_i \\ \dot{v}_i &= a_i \\ x_i &= \sum_{n=0}^5 b_{n_i} \cdot s_i^n \\ y_i &= \sum_{n=0}^5 c_{n_i} \cdot s_i^n \end{aligned} \quad (3)$$

Where a_i is the longitudinal acceleration of traffic object i . This accelerations of all traffic objects are assumed to be constant during for the duration of the prediction horizon. The state X_{ego} of the ego-vehicle is:

$$X_{ego} \in \mathbb{R}^5 = \begin{pmatrix} s_{ego} \\ v_{ego} \\ x_{ego} \\ y_{ego} \\ \theta_{ego} \end{pmatrix}$$

Where v_{ego} is the longitudinal velocity, x_{ego} is the global x-coordinate, y_{ego} is the global y-coordinate, and θ_{ego} is the yaw angle of the ego-vehicle. The transition model describing the ego vehicle is:

$$\begin{aligned} \dot{s}_{ego} &= v_{ego} \\ \dot{v}_{ego} &= u_{cntrl} \\ x_{ego} &= \sum_{n=0}^5 b_{n_{ego}} \cdot s_{ego}^n \\ y_{ego} &= \sum_{n=0}^5 c_{n_{ego}} \cdot s_{ego}^n \\ \theta_{ego} &= \sum_{n=0}^5 d_{n_{ego}} \cdot s_{ego}^n \end{aligned} \quad (4)$$

Where u_{cntrl} is the control input that is optimized.

In order to guarantee safe, legal and comfortable driving behavior, a set of constraints has been placed on the transition model. The most important set of constraints has the goal to avoid collisions between the ego-vehicle and surrounding vehicles. To achieve this, a safety ellipse is generated around the ego-vehicle that encompasses an area with the width of the ego-vehicle and a distance in front of the vehicle approximately equal to a two second following distance, which follows the yaw angle of the ego-vehicle. This safety ellipse is shown in figure 3. The constraints prohibit traffic objects from entering the safety ellipse. In order to increase robustness of the controller, it is important to include a slack variable, as proposed in [25], in these constraints. This makes sure that, even when the constraints are broken, an optimal control input can be calculated. The constraint to prevent collisions between the ego-vehicle and traffic object i is shown in equation (5).

$$\begin{aligned} & \frac{((x_i - x_{ego} - x_t) \cos \theta_{ego} + (y_i - y_{ego} - y_t) \sin \theta_{ego})^2}{d_{trail}^2} \\ & + \frac{((x_i - x_{ego}) \sin \theta_{ego} - (y_i - y_{ego}) \cos \theta_{ego})^2}{d_{width}^2} \\ & + \epsilon_i \geq 1 \end{aligned} \quad (5)$$

Where:

$$\begin{aligned} x_t &= \frac{1}{2} t_{trail} \cdot v_{ego} \cdot \cos \theta_{ego} \\ y_t &= \frac{1}{2} t_{trail} \cdot v_{ego} \cdot \sin \theta_{ego} \\ d_{trail} &= t_{trail} \cdot v_{ego} + d_{length} \end{aligned}$$

And t_{trail} is the desired trailing time ahead of the ego-vehicle, d_{width} is the width of the ego-vehicle, d_{length} is the length of the ego-vehicle, and ϵ_i is the slack variable.

Besides the safety constraints, the MPC makes use of a constraint on the maximum velocity of the ego-vehicle. In order to prevent the ego-vehicle from severely breaking legal speed limits, a constraint is placed that limits the maximum velocity of the ego-vehicle to 5% above the target speed that is included in the digital map. Another slack variable is included on this constraint. This allows the controller to break the speed limit to avoid collisions in a worst case scenario. Additionally, a constraint is placed on the minimum velocity of the ego-vehicle. Limiting the minimum velocity to 0 m s^{-1} prevents the controller from deciding the vehicle has to reverse.

Furthermore, constraints are placed on the maximum allowed acceleration and deceleration. In this MPC the choice is made to limit the acceleration to a maximum value of 2 m s^{-2} and to limit the deceleration to -2.5 m s^{-2} . These constraints are based on the technical limitation of the simulated vehicle. By placing the acceleration and deceleration limits at higher values, the acceleration optimized by the MPC cannot be directly followed by the simulated vehicle, which could result in undesirable actions.

The cost function h of the MPC is set up as a least squares function. In the least squares function, the distance between a variable and its reference value is squared, multiplied by a weight w and summed. In the cost function, shown in equation (6) a cost is placed on the longitudinal velocity v_{ego} with it's reference value of the target velocity v_{ref} . Furthermore,

a cost is placed on the acceleration a_{ego} , with the goal to maximize comfort inside the ego-vehicle. Lastly, a cost is placed on the slack variables ϵ_{ij} to discourage breaking the safety constraints.

$$h = \sum_{j=1}^{N_H} \sum_{i=1}^{N_{\text{objs}}} w_v \left\| v_{\text{ego}_j} - v_{\text{ref}} \right\|^2 + w_a a_{\text{ego}_j}^2 + w_i \epsilon_{ij}^2 \quad (6)$$

The optimization problem is solved using QPOASES. This open source implementation for solving quadratic programming (QP) has shown to outperform many other QP-solvers and has a direct interface with the ACADO toolkit [26]. The optimization is iterated 10 times to minimize the integration error, and the entire process of situation analysis and behavior planning is iterated every 0.2s of the simulation. The choice to sample a longitudinal control input every 0.2s is based on a study by Aldert as cited in [10]. The study found that "In order to guarantee a reactive behavior, the decision making process has to be performed with a sampling period of at [most] $\Delta T = 0.2$ seconds."

IV. SIMULATION RESULTS

To test and validate the performance of the newly developed behavior planning module, a number of urban driving scenarios are simulated. The behavior planning module controls the longitudinal acceleration of a Mercedes-Benz ML SUV with automatic transmission. The simulations are performed on three different intersections. These intersections are: a large single lane roundabout, a straight 4-way intersection and a small Y-intersection. For each of the three simulated intersections, a variety of initial conditions and traffic object trajectories are tested. As discussed in section II-A, the performance of the behavior planning module will be judged on safety, comfort and time efficiency.

During initial testing of the behavior planning module, a number of parameters are determined. With these parameters, shown in Table II, the performance during initial testing was found to be acceptable.

Parameter	Value
Prediction horizon t_H	5 s
Trailing time t_{trail}	1.9 s
Number of prediction steps N_H	15
Number of optimization iterations	10
Maximum number of traffic objects	4
Width of ego-vehicle d_{width}	1.85 m
Length of ego-vehicle d_{length}	5 m
Cost weight on velocity w_v	1
Cost weight on acceleration w_a	10
Cost weight on velocity slack $w_{\epsilon,v}$	10^4
Cost weight on safety slack $w_{\epsilon,i}$	10^4

Table II: Model parameters for traffic simulations.

A. Roundabout

The roundabout intersection consists of a large single-lane roundabout. Three different roundabout scenarios are

simulated, each with slightly different behavior of traffic objects. For each of the scenarios, the ego-vehicle approaches the roundabout with a speed of 8.3 m s^{-1} (30 km h^{-1}), while two traffic objects are occupying the roundabout. In the first scenario, the two traffic objects follow each other closely, preventing the ego-vehicle to merge between the traffic objects. In the second scenario, the gap between the traffic objects is larger, allowing for the possibility that the ego vehicle merges between the traffic objects. In the third scenario, the second traffic object follows the other traffic object closely, after which it exits the roundabout ahead of the ego-vehicle.

1) *Roundabout scenario 1*: In this scenario, both traffic objects continue on the roundabout, and the ego-vehicle enters the roundabout. Both traffic objects have an initial velocity of 8.3 m s^{-1} , and maintain this velocity for the duration of the simulation. The maneuver prediction model correctly predicts that both traffic objects keep following the roundabout and do not make a right turn.

Figure 5 shows the velocity profile, acceleration and jerk of the ego vehicle during the scenario. The initial velocity of the ego vehicle is 8.3 m s^{-1} , and this velocity is maintained until approximately 3 seconds after the start of the simulation. At that moment, the ego vehicle starts decelerating with approximately -0.65 m s^{-2} . Figure 4a shows the scene at 6 seconds after the start of the simulation. At that moment, the two traffic objects are approaching the roundabout exit at constant velocity, with the ego vehicle decelerating its approach to the roundabout entrance. At $t = 8 \text{ s}$, the deceleration of the ego vehicle is shortly increased to a maximum deceleration of -1.82 m s^{-2} . At approximately $t = 9.5 \text{ s}$, the vehicle shifts gears, resulting in large spikes in the acceleration profile. Figure 4b shows the scene at $t = 10 \text{ s}$. At that moment, traffic object 1 has passed the roundabout exit, with traffic object 2 in the middle of the roundabout exit. After the gearshift, the ego vehicle shortly decelerates with -1.5 m s^{-2} until the vehicle reaches a minimum velocity of 1 m s^{-1} at $t = 12 \text{ s}$. Figure 4c shows the scene at that time instance. At that moment, the two traffic objects have passed the roundabout exit, and the ego vehicle starts to accelerate with a maximum value of 1.1 m s^{-2} onto the roundabout. The vehicle continues to accelerate until the end of the simulation, just before it has reached its target speed of 8.3 m s^{-1} .

The closest distance between the ego-vehicle and any of the traffic objects occurs at $t = 11 \text{ s}$. At that moment the distance between the centers of the ego-vehicle and traffic object 2 is 6.2m. At that moment, the ego-vehicle has a speed of only 1 m s^{-1} . This equates to an inter-vehicle time of $\text{TIV} = 6.2 \text{ m}$, however at these velocities the absolute distance is a better indicator of safety than the inter-vehicle time. With a maximum deceleration of -1.82 m s^{-2} , and a maximum acceleration of 1.1 m s^{-2} , the driving behavior is just outside the acceptable levels as discussed in section II-A. More comfortable driving behavior could have been achieved if the vehicle decelerated slightly harder in the earlier stages of the approach to the roundabout, however this conflicts with the aim of the controller to maintain the highest allowed

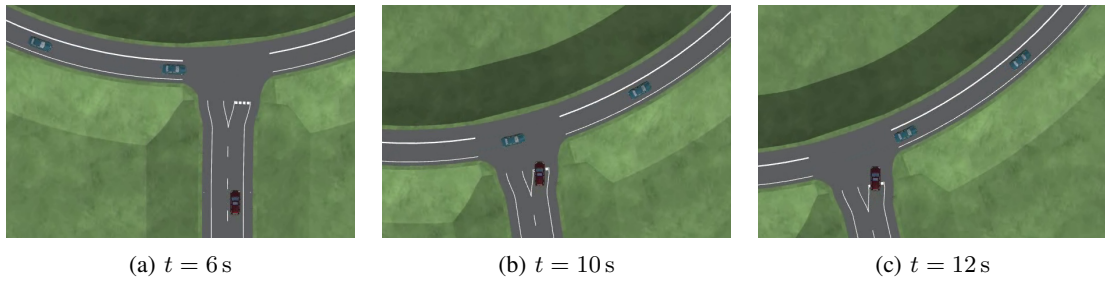


Figure 4: Snapshots of scenario 1 on the roundabout. The ego-vehicle approaches the roundabout with two traffic objects present on the roundabout. The ego-vehicle decelerates to enter the roundabout behind the two traffic objects.

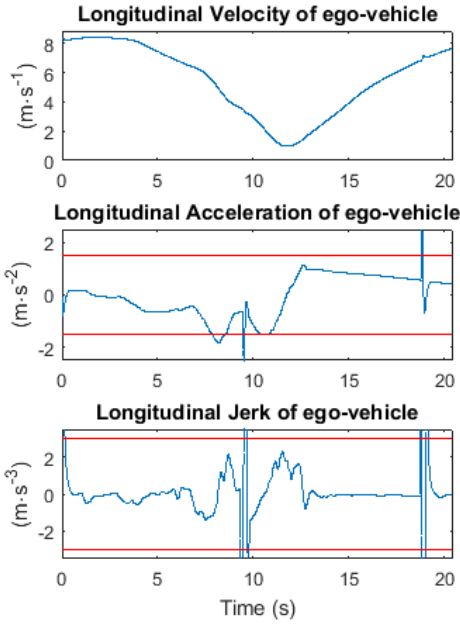


Figure 5: Longitudinal velocity, acceleration and jerk of the ego-vehicle in scenario 1 on the roundabout. The spikes in the acceleration and jerk are the result of gearshifts of the automatic transmission. The horizontal lines indicate comfort limits.

velocity. The longitudinal jerk of the ego-vehicle only exceeds the comfort limits during gearshifts. As these gearshifts are controlled by the automatic transmission, the peak acceleration and jerk during the gearshifts is not attributed to the behavior planning module. The highest absolute peak value that can be attributed to the behavior planner is 2.3 m s^{-3} and occurs at $t = 11.5 \text{ s}$. The TTI for this scenario is 1.6 s , which means the ego-vehicle has joined the intersection relatively quickly after being vacated by the traffic objects.

2) *Roundabout scenario 2*: In this scenario, the first traffic object, TO1, has identical initial conditions as in scenario 1, and follows the same path. Traffic object 2, TO2, follows

the other traffic object at a longer distance as compared to scenario 1. The maneuver prediction module is correctly able to predict that both traffic objects continue their trajectory on the roundabout.

Figure 7 shows the longitudinal velocity profile of the two traffic objects. Both vehicles travel at a constant velocity of 8.3 m s^{-1} . However, after the ego-vehicle has merged between the two traffic objects at $t = 11 \text{ s}$, traffic object 2 slightly reduces its velocity to maintain a safe following distance to the ego-vehicle.

Figure 8 shows the longitudinal velocity, acceleration and jerk of the ego-vehicle. The ego-vehicle travels at an initial velocity of 8.3 m s^{-1} , and maintains this velocity for the first 3 seconds of the simulation. Between $t = 3 \text{ s}$ and $t = 7.5 \text{ s}$, the ego-vehicle reduces its velocity with a maximum deceleration of -0.7 m s^{-2} . Figure 6a shows the scene at $t = 7 \text{ s}$. At that moment, traffic object 1 is just passing the roundabout exit, with the ego-vehicle approaching the entrance to the roundabout. Between $t = 7.5 \text{ s}$ and $t = 10 \text{ s}$, the ego-vehicle maintains a somewhat constant velocity, before entering the turn to join the roundabout. Figure 6b shows the scene at $t = 10 \text{ s}$. At that moment, traffic object 1 has passed the roundabout exit and traffic object 2 is far enough back for the ego-vehicle to merge in between the traffic objects. During cornering, the ego-vehicle scrubs some of its velocity, resulting in a peak deceleration of -1.6 m s^{-2} . After completing the corner to join the roundabout, the vehicle starts to accelerate back up to its target velocity of 8.3 m s^{-1} , with a peak acceleration of 0.7 m s^{-2} . Figure 6c shows the scene at $t = 12 \text{ s}$. At that moment, the ego-vehicle has joined the roundabout between the two traffic objects.

The closest distance between the ego-vehicle and any of the traffic objects occurs at $t = 9 \text{ s}$. At that moment, the distance between the ego-vehicle and traffic object 1 is 12.5 m with the ego-vehicle traveling with a velocity of 6.4 m s^{-1} . This equates to an inter-vehicle time of $\text{TIV} = 1.95 \text{ s}$, which is approximately equal to the recommended safety distance as discussed in section II-A. With a peak deceleration of -1.6 m s^{-2} and a maximum acceleration of 0.7 m s^{-2} , this driving behavior is just outside of the acceptable margins. Because the largest peak in deceleration originates from cornering, higher comfort levels can be achieved by reducing

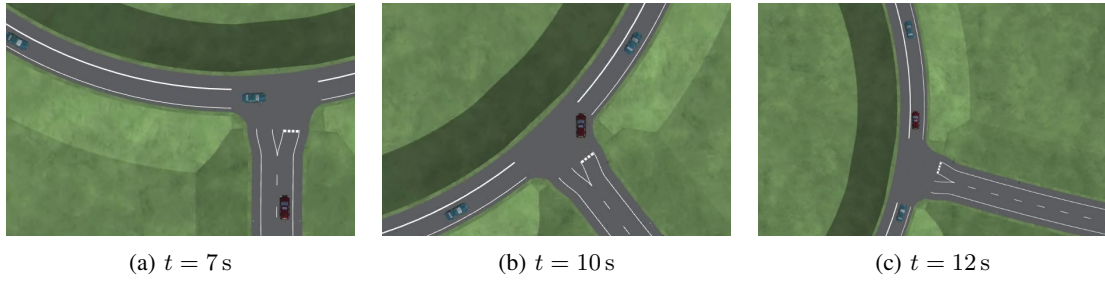


Figure 6: Snapshots of scenario 2 on the roundabout. The ego-vehicle approaches the roundabout with two traffic objects present. Because of the larger gap between the traffic objects, the ego-vehicle is able to merge in between.

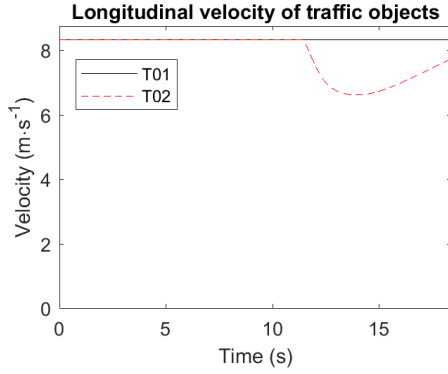


Figure 7: Longitudinal velocity of traffic objects in scenario 2 on the roundabout. Traffic object 1 maintains its initial velocity, with traffic object 2 decelerating slightly to maintain a safe distance.

the target velocity before the start of the corner. The longitudinal jerk levels stay well within the comfort limits. The maximum absolute jerk is 2.5 m·s^{-3} , and occurs at $t = 11.2 \text{ s}$. The TTI for this scenario is 1.3 s , which means the ego-vehicle has joined the intersection relatively quickly after being vacated by the traffic objects.

3) *Roundabout scenario 3*: In this scenario, traffic object 1 has identical initial conditions as in scenario 1 and 2 of the roundabout, and follows the same path. Traffic object 2 has identical initial conditions as in scenario 1 of the roundabout, however, in contrast to scenario 1, traffic object 2 makes a right turn exiting the roundabout.

Figure 10 shows the velocity profiles of the two traffic objects. Traffic object 1 travels at a constant velocity of 8.3 m·s^{-1} . Traffic object 2 has the same initial velocity but reduces its speed slightly to maintain a safe following distance to traffic object 1. At $t = 6 \text{ s}$, traffic object 2 decelerates before exiting the roundabout. At that same moment, the maneuver prediction module is able to predict that traffic object 2 will make a right turn at the roundabout exit. After exiting the roundabout, traffic object two accelerates back up to its initial velocity of 8.3 m·s^{-1} .

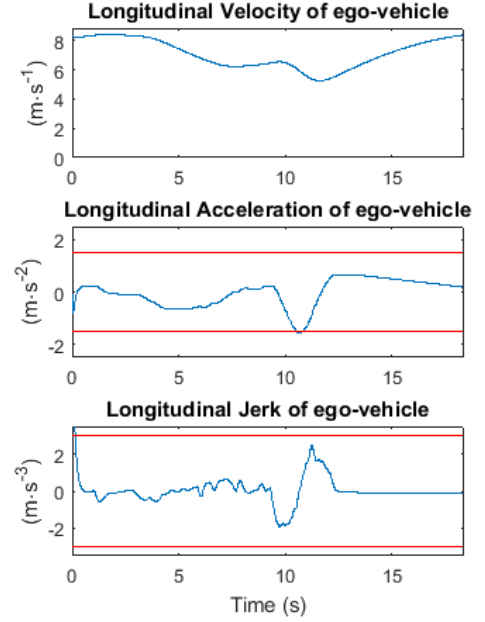


Figure 8: Longitudinal velocity, acceleration and jerk of the ego-vehicle in scenario 2 on the roundabout. The horizontal lines indicate comfort limits.

As is shown in figure 11, the longitudinal velocity, acceleration and jerk profiles of the ego-vehicle during this scenario are nearly identical to those of scenario 2 shown in figure 8. This shows that the behavior planning module efficiently uses the predicted maneuver to predict that the path of traffic object 2 will not coincide with the path of the ego-vehicle, resulting in similar behavior as to when traffic object 2 was at a larger distance behind traffic object 1.

Figures 9a through 9c show the scenes at $t = 7 \text{ s}$, $t = 9 \text{ s}$ and $t = 12 \text{ s}$. From this, it is clear that the ego vehicle is able to predict early on that traffic object 2 will exit the roundabout and adjusts its behavior only on the presence of traffic object 1.

The closest distance between the ego-vehicle and any of the traffic objects occurs at $t = 9 \text{ s}$. At that moment, the distance

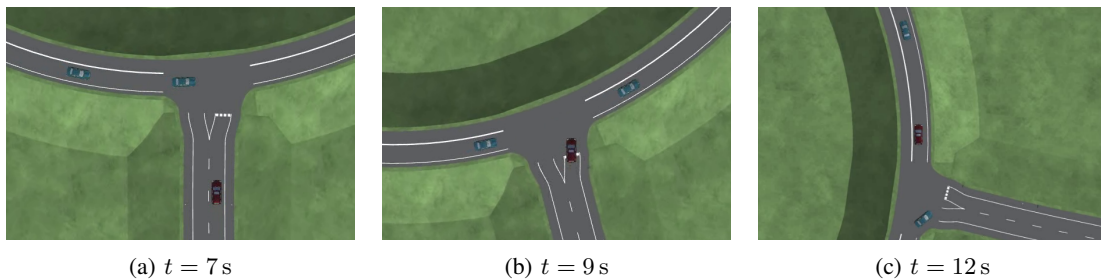


Figure 9: Snapshots of scenario 3 on the roundabout. The ego-vehicle approaches the roundabout with two traffic objects present. Traffic object 1 maintains its trajectory on the roundabout. Because traffic object 2 is predicted to exit the roundabout, the ego-vehicle merges onto the roundabout in front of traffic object 2.

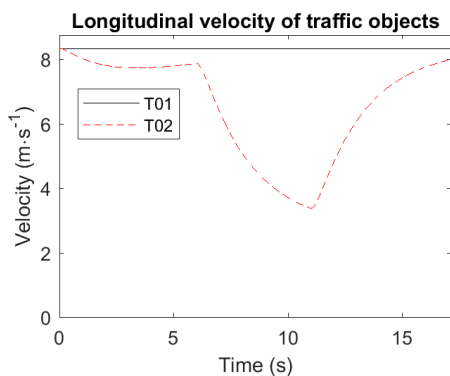


Figure 10: Longitudinal velocity of the traffic objects in scenario 3 on the roundabout. Traffic object 1 maintains its initial velocity, with traffic object 2 reducing its velocity prior to exiting the roundabout.

between the ego-vehicle and traffic object 1 is 12.6 m, with the ego-vehicle traveling at 6.3 m s^{-1} . This equates to an inter-vehicle time of exactly 2 seconds, which is the recommended minimum distance between vehicles. The maximum deceleration of the ego vehicle is an acceptable -1.5 m s^{-2} . The jerk levels are well within the comfort limits, with a maximum longitudinal jerk of 2.4 m s^{-3} , which occurs at $t = 11.2 \text{ s}$. The TTI for this scenario is 1.3 s, which means the ego-vehicle follows traffic object 1 in the same way it did in scenario 2 on the roundabout.

B. Straight four-way Intersection

The straight four-way intersection consists of four connecting roads, each with a length of 100 m. In each simulated scenario the ego-vehicle approaches this intersection with a speed of 13.9 m s^{-1} (50 km h^{-1}). For each scenario, three traffic objects are present and approaching the intersection from the right. The subsequent behavior of the three traffic objects is varied between the scenarios. For this intersection, two scenarios are simulated. In the first scenario, the three traffic objects maintain a straight trajectory across

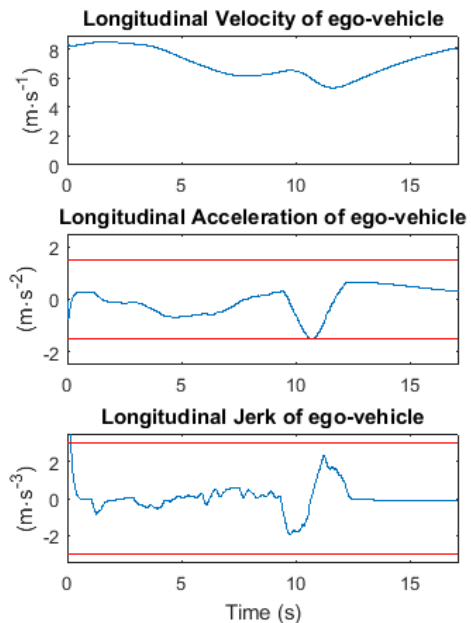


Figure 11: Longitudinal velocity, acceleration and jerk of the ego-vehicle in scenario 3 on the roundabout. The horizontal lines indicate comfort limits.

the intersection, forcing the ego-vehicle to adapt its velocity to avoid a collision. In the second scenario, one of the traffic objects makes a right turn on the intersection, which tests the maneuver prediction ability of the behavior planning module.

1) *Four-way scenario 1*: In scenario 1 of the four-way intersection, three traffic objects approach the intersection from the right. The first two traffic objects maintain a speed of 13.9 m s^{-1} , with the third traffic object following at a speed of 11.1 m s^{-1} . Throughout the scenario, the maneuver prediction module is able to correctly predict that the three traffic objects will go straight on the intersection. The progression of the scenario is shown in Figures 12a through 12c.

Figure 13 shows the velocity, acceleration and jerk profile

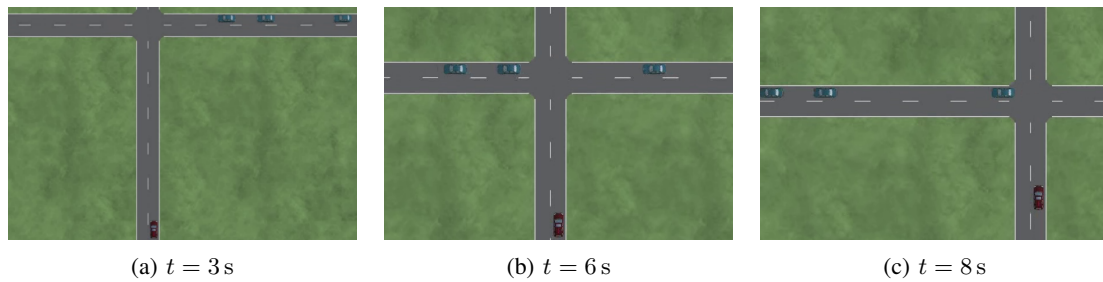


Figure 12: Snapshots of scenario 1 on the four-way intersection. The ego-vehicle approaches the intersection with three traffic objects coming from the right. The ego-vehicle decelerates to let the traffic objects through before entering the intersection.

of the ego-vehicle. The initial velocity of the ego-vehicle is 13.9 m s^{-1} , which it maintains for approximately 1 second. At $t = 1 \text{ s}$, the ego-vehicle recognizes that it needs to decelerate to avoid a collision with the traffic objects. Figure 12a shows the scenario at $t = 3 \text{ s}$, where the first traffic object is about to enter the intersection. At that moment, the ego-vehicle is decelerating with a rate of -1.3 m s^{-2} . The deceleration is increased until the peak deceleration of -2.3 m s^{-2} is achieved. At $t = 6 \text{ s}$, the first two traffic objects have passed the intersection, and the deceleration of the ego-vehicle is slightly reduced. At $t = 6.8 \text{ s}$ and $t = 7.7 \text{ s}$, the automatic gearbox makes two downshifts resulting in peaks in deceleration and jerk that are not attributed to the behavior planning module. At $t = 8 \text{ s}$, the third traffic object has passed the intersection. After that moment, the ego-vehicle starts to accelerate back up to the target velocity with a peak acceleration of 1.2 m s^{-2} .

The closest distance between the ego-vehicle and any of the traffic objects occurs at $t = 7.9 \text{ s}$ when traffic object 3 is in the middle of the intersection. At that moment, the distance between the ego-vehicle and traffic object 3 is 19.9 m , while the ego-vehicle travels at a speed of 3 m s^{-1} . This distance is quite a bit larger than necessary, which results in decelerations that are higher than optimal. The peak deceleration is -2.3 m s^{-2} which is more than 50% higher than the acceptable limit proposed in Section II-A. Excluding the peaks in jerk due to the automatic gearshift, the jerk stays within the comfort limits with a maximum value of 2.6 m s^{-3} . The TTI for this scenario is 2.5 s , which means the ego-vehicle has joined the intersection relatively quickly after being vacated by the traffic objects.

2) *Four-way scenario 2*: The second scenario of the four-way intersection consists of the first and third traffic objects going straight, with the second traffic object making a right turn. Figures 14a through 14c show the progression of the scenario during the simulation, with Figure 15 showing the velocity profiles of the traffic objects. Traffic object 1 maintains a constant velocity of 13.9 m s^{-1} for 8 seconds, until it has passed clear of the intersection, after which it quickly slows down to near standstill. The reason for this is that this map for the intersection has roads of only 100 m leading up to it. Unfortunately the way the simulation software is set up causes

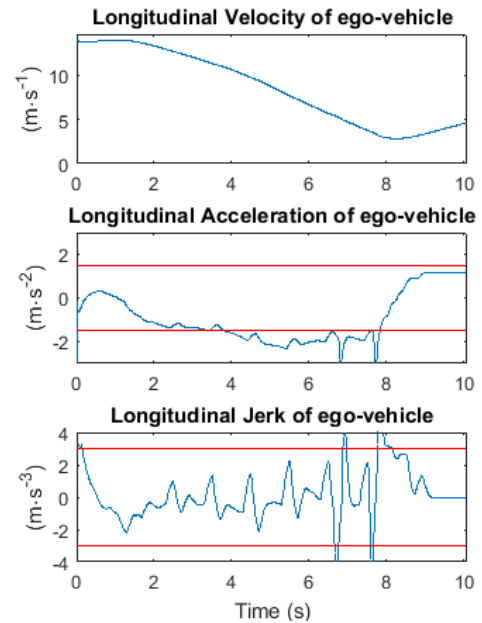


Figure 13: Longitudinal velocity, acceleration and jerk of the ego-vehicle in scenario 1 on the four-way intersection. The spikes in acceleration and jerk are the result of gearshifts of the automatic transmission. The horizontal lines indicate comfort limits.

errors when traffic objects exceed the limitations of the map. Therefore, all traffic objects come to a halt before this moment. Traffic object two starts with the same constant velocity of 13.9 m s^{-1} . After approximately two seconds, the vehicle starts decelerating until it reaches 4.8 m s^{-1} , after which it makes a right turn and accelerates back up to 13.9 m s^{-1} . Traffic object 2 starts with the same velocity of 13.9 m s^{-1} , and quickly decelerates to keep a safe following distance to the vehicle in front. After traffic object 2 makes the turn right, traffic object 3 accelerates shortly, and slows down again to avoid the first traffic object.

For traffic objects 1 and 3, the maneuver prediction module correctly predicts that these vehicles will maintain a straight

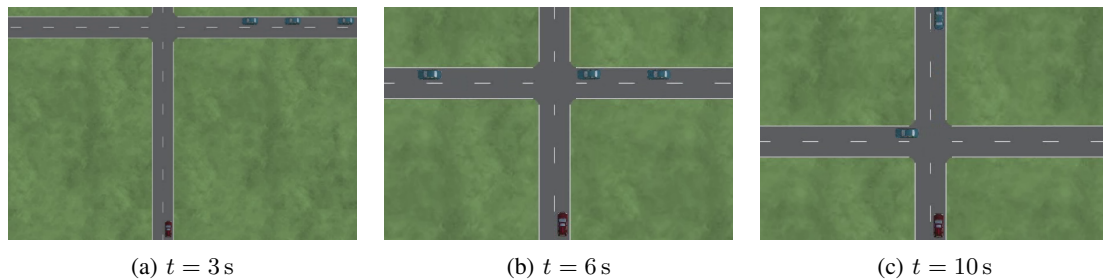


Figure 14: Snapshots of scenario 2 on the four-way intersection. The ego-vehicle approaches the intersection with three traffic objects coming from the right. The first and third traffic object go straight over the intersection, with traffic object 2 making a right turn. The ego-vehicle decelerates to let the traffic objects through before entering the intersection.

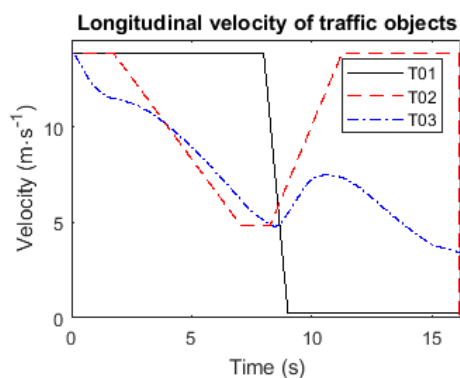


Figure 15: Longitudinal velocity of the traffic objects in scenario 2 on the four-way intersection. Traffic object 1 maintains its initial velocity for 8 seconds after which it reduces its velocity to avoid exiting the map. Traffic object 2 slows down before entering the intersection. After making a right turn, the traffic object accelerates. Traffic object 3 maintains adjusts its velocity to maintain a safe distance to the other traffic objects.

trajectory over the intersection. For traffic object 2, after approximately 4 seconds, the maneuver prediction module predicts that the vehicle will turn right at the intersection.

Figure 16 shows the longitudinal velocity, acceleration and jerk profiles of the ego-vehicle. The ego-vehicle has an initial velocity of 13.9 m s^{-1} , which it maintains for the first second of the simulation. After approximately 1 second, the ego-vehicle starts decelerating, and continuous to do so until $t = 10 \text{ s}$, where the vehicle is momentarily at standstill. Figure 14a shows that at $t = 3 \text{ s}$, the three traffic objects are still approaching the intersection. At $t = 4.4 \text{ s}$, a peak deceleration of -2.3 m s^{-2} is achieved. Figure 14b shows that at $t = 6 \text{ s}$, traffic object 1 has vacated the intersection, with traffic object 2 on the verge of entering the roundabout and making a right turn. At approximately $t = 7 \text{ s}$ and $t = 8 \text{ s}$, two peaks occur in the acceleration and jerk profiles of the ego-vehicle. These peaks are the result of downshifts of the automatic gearbox and are not attributed to the behavior planner. Figure 14c shows the

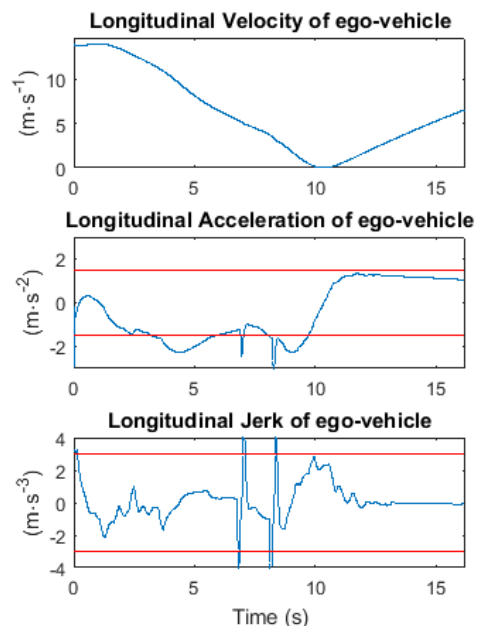


Figure 16: Longitudinal velocity, acceleration and jerk of the ego-vehicle in scenario 2 on the four-way intersection. The spikes in acceleration and jerk are the result of gearshifts of the automatic transmission. The horizontal lines indicate comfort limits.

scenario at $t = 10 \text{ s}$. At that moment, traffic object 3 has passed the intersection, and the behavior planning module determines that the path is clear, which results in acceleration of the ego-vehicle.

The minimum distance between the ego-vehicle and the traffic objects is 17.1 m at 10 seconds after the start of the simulation. At that moment, the ego vehicle is at standstill, therefore this is considered to be a very safe maneuver. The maximum deceleration of the vehicle is found to be -2.3 m s^{-2} and occurs at both $t = 4.4 \text{ s}$, and $t = 9.0 \text{ s}$. This is 50% over the acceptable acceleration level. A more comfortable behavior could have been reached by maintaining a

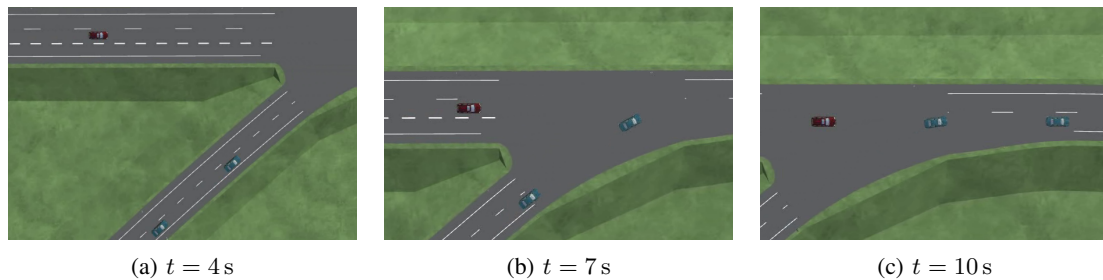


Figure 17: Snapshots of scenario 1 on the Y-intersection. The ego-vehicle approaches the Y-intersection, with two traffic objects approaching the intersection from the other road, following each other closely. The ego-vehicle decelerates to merge onto the intersection behind both traffic objects, maintaining a safe following distance.

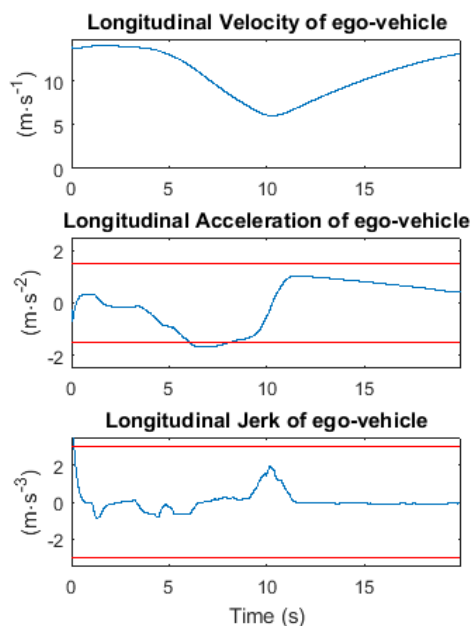


Figure 18: Longitudinal velocity, acceleration and jerk of the ego-vehicle in scenario 1 on the Y-intersection. The horizontal lines indicate comfort limits.

smaller distance to traffic object 3. The jerk of the ego-vehicle remains within the comfort limits with a maximum value of $2.8 \text{ m}\cdot\text{s}^{-3}$. The TTI for this scenario is 4.1 s, which means the ego-vehicle waits quite a long time before joining the intersection. This is likely due to the ego-vehicle completely coming to a stop to avoid colliding with the traffic objects.

C. Y-intersection

The Y-intersection scenarios consist of the ego-vehicle approaching a Y-intersection at approximately the same time as two traffic objects that follow each other. On this intersection, the traffic objects and ego-vehicle merge together onto one single road. The only available maneuver for all

vehicles on this intersection is to go straight through the junction. Two scenarios are evaluated on the Y-intersection. In the first scenario, the two traffic objects follow each other closely leaving little space for the ego-vehicle to merge in between, which forces the ego-vehicle to adapt its driving behavior. In the second scenario, the two traffic objects follow each other at a longer distance, allowing the ego-vehicle to merge between the two traffic objects after adjust its velocity.

1) *Y-intersection scenario 1*: In this scenario, two traffic objects approach the Y-intersection on the same road following each other closely, with the ego-vehicle approaching the intersection on the other road. Figure 17a shows the state of the scenario at $t = 4 \text{ s}$. Both traffic objects approach the intersection with a velocity of $13.9 \text{ m}\cdot\text{s}^{-1}$, and maintain that velocity for the duration of the scenario. The ego-vehicle approaches the intersection with the same velocity, but is forced to adjust its velocity to avoid colliding with the traffic objects.

Figure 18 shows the longitudinal velocity, acceleration and jerk of the ego-vehicle. The ego-vehicle maintains its initial velocity of $13.9 \text{ m}\cdot\text{s}^{-1}$ for the first 4 seconds of the simulation. At approximately $t = 4 \text{ s}$, shown in Figure 17a, the ego-vehicle starts to decelerate to allow the traffic objects to merge in front of the ego-vehicle. The deceleration is increased until a peak deceleration of $-1.7 \text{ m}\cdot\text{s}^{-2}$ is achieved at $t = 7 \text{ s}$. As is shown in Figure 17b, at that moment traffic object 1 has passed the intersection with both traffic object 2 and the ego-vehicle about to enter the intersection. From $t = 7 \text{ s}$ the vehicle reduces the deceleration until the minimal velocity of $6 \text{ m}\cdot\text{s}^{-1}$ is reached at $t = 10 \text{ s}$. Figure 17c shows that, at that moment, both traffic objects have passed the intersection, and the ego-vehicle is able to follow traffic object 2. The ego-vehicle then accelerates back up to its target velocity of $13.9 \text{ m}\cdot\text{s}^{-1}$ with a peak acceleration of $1 \text{ m}\cdot\text{s}^{-2}$ occurring at $t = 12 \text{ s}$.

The closest distance between the ego-vehicle and any of the traffic objects occurs at $t = 9 \text{ s}$. At that moment, the distance between the ego-vehicle and traffic object 2 is 15 m, and the velocity of the ego-vehicle is $7.2 \text{ m}\cdot\text{s}^{-1}$. This equates to an inter-vehicle time of just over 2 seconds, indicating that the driving behavior can be considered safe.

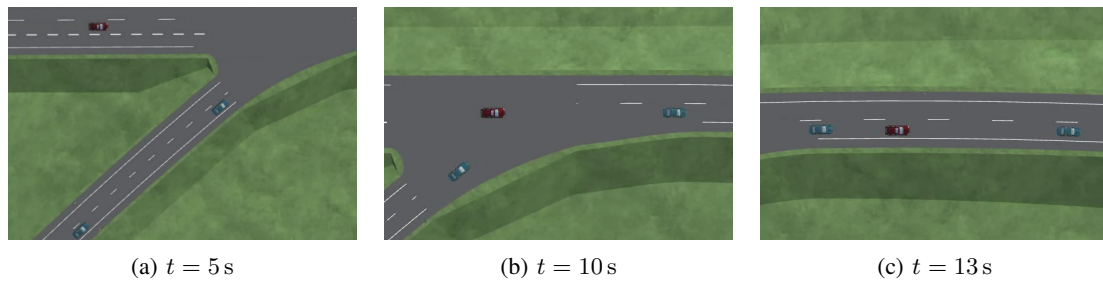


Figure 19: Snapshots of scenario 2 on the Y-intersection. The ego-vehicle approaches the Y-intersection, with two traffic objects approaching the intersection from the other road with a slight gap between the traffic objects. The ego-vehicle decelerates to let traffic object 1 enter the intersection first. Thereafter, the ego-vehicle accelerates to merge onto the intersection between both traffic objects, while maintaining a safe following distance to traffic object 1.

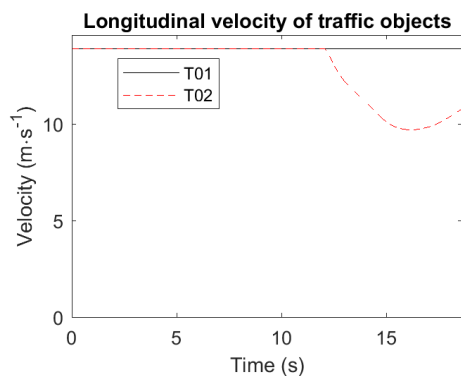


Figure 20: Longitudinal velocity of the traffic objects in scenario 2 on the Y-intersection. Traffic object 1 maintains its initial velocity. Traffic object 2 only adjusts its velocity after passing the intersection, to maintain a safe following distance to the ego-vehicle.

With a peak acceleration of 1 m s^{-2} and a peak deceleration of -1.7 m s^{-2} , the driving behavior is slightly outside the acceleration limits proposed in [20]. The longitudinal jerk stays well within the comfort limits for the duration of the simulation, with a peak jerk of 1.9 m s^{-3} , occurring at $t = 10.2 \text{ s}$. The TTI for this scenario is 1.6 s , which means the ego-vehicle has joined the intersection relatively quickly after being vacated by the traffic objects.

2) *Y-intersection scenario 2*: In this scenario the distance between the two traffic objects is slightly bigger as compared to the previous scenario. The velocity profiles of the traffic objects are shown in Figure 20. Both traffic objects have an initial velocity of 13.9 m s^{-1} . Traffic object 1 maintains this velocity for the duration of the scenario. Traffic object 2 is programmed to maintain its initial velocity until it has passed the intersection at $t = 12 \text{ s}$, after which it adjusts its velocity to maintain a safe gap to the vehicle in front. This is done to force the ego-vehicle to adjust its behavior to the traffic objects, instead of relying on the traffic objects to create space

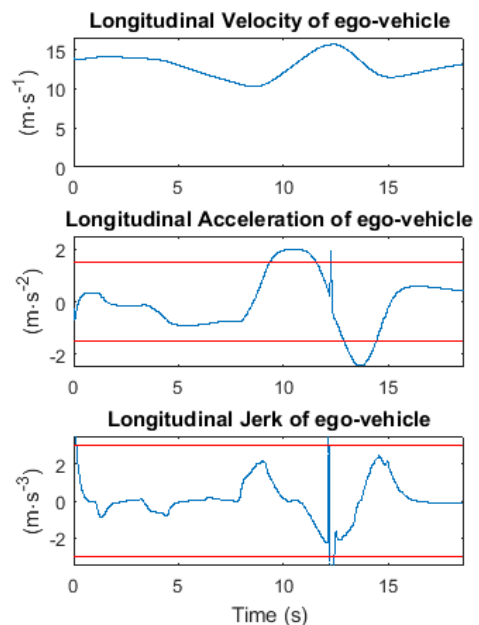


Figure 21: Longitudinal velocity, acceleration and jerk of the ego-vehicle in scenario 2 on the Y-intersection. The spikes in the acceleration and jerk are the result of gearshifts of the automatic transmission. The horizontal lines indicate comfort limits.

for the ego-vehicle.

Figure 21 shows the longitudinal velocity, acceleration and jerk profiles of the ego-vehicle. The vehicle has an initial velocity of 13.9 m s^{-1} and maintains this velocity for the initial 3.5 s . From that moment until $t = 8.5 \text{ s}$, the ego-vehicle decelerates with a peak of -0.9 m s^{-2} . Figure 19a shows the state of the scenario at $t = 5 \text{ s}$. At that moment, traffic object 1 enters the roundabout. Traffic object 2 follows the other traffic object at a distance, and the ego-vehicle is decelerating to allow traffic object 1 to join the intersection. At $t = 8.5 \text{ s}$, the ego-vehicle achieves the minimum velocity of 10.3 m s^{-1} ,

after which the vehicle starts to accelerate. At $t = 10$ s, traffic object 1 has passed the intersection, the ego-vehicle is in the middle of the intersection, and traffic object 2 is starting to join the intersection, as shown in Figure 19b. At that moment the ego-vehicle reaches its maximum acceleration of 2 m s^{-2} which it maintains for a second, after which the vehicle reduces its acceleration. At approximately $t = 12$ s, the ego-vehicle makes a gearshift, explaining the sudden spike in acceleration. At that moment, the ego-vehicle reaches a maximum velocity of 15.7 m s^{-1} . This means that the vehicle slightly exceeds its target velocity in order to increase the gap to traffic object 2 behind. At $t = 13$ s, shown in Figure 19c, the traffic objects have passed the intersection, and the ego-vehicle is now in between the two traffic objects. At that moment, traffic object 2 is reducing its velocity to maintain a safe distance to the ego-vehicle, and the ego-vehicle decelerates strongly to maintain a safe distance to traffic object 1. The ego-vehicle reaches a peak deceleration of -2.4 m s^{-2} at $t = 13.7$ s, until it reaches a velocity of 11.5 m s^{-1} , after which it slowly accelerates back up to the target velocity of 13.9 m s^{-1} .

The closest distance between the ego-vehicle and any of the traffic objects occurs at $t = 11$ s. At that moment, the ego-vehicle is ahead of traffic object 2, with traffic object 2 closely following the ego-vehicle at a distance of 10.3 m. This distance is quickly increased by the acceleration of the ego-vehicle, and slight deceleration of the traffic object. At $t = 12$ s, the ego-vehicle is following traffic object 1 at a distance of 31.3 m while driving with a velocity of 15.7 m s^{-1} . This equates to an inter-vehicle time of approximately 2 seconds, indicating that the following distance to traffic object 1 is safe. During the scenario, the ego-vehicle achieves a peak deceleration of -2.4 m s^{-2} and a peak acceleration of 2 m s^{-2} . Both these values exceed the limits proposed in [20] considerably. However, the jerk levels stay well within the comfort limits, with a maximum jerk of 2.5 m s^{-3} , occurring at $t = 14.6$ s. The TTI for this scenario is 2.5 s, which means the ego-vehicle has joined the intersection relatively quickly after being vacated by the traffic objects.

D. Discussion of Results

The results of the simulations are summarized in Table III, where the minimum distances and inter-vehicle time (TIV), the peak acceleration and jerk values, and the time to intersection (TTI) are shown for each scenario. For all the tested scenarios, the maneuver prediction module was able to correctly predict the maneuvers of the traffic objects. With these maneuver predictions, the behavior planning module was able to maintain a safe distance to the traffic objects through all the tested scenarios. Only in scenario 2 on the roundabout, the inter-vehicle time momentarily drops to 1.95 s. The most important factor in determining driving comfort is jerk. For all scenarios, the peak longitudinal jerk remains well under the comfort limit of 3 m s^{-3} . However, in nearly all the tested scenarios, the peak longitudinal acceleration slightly exceeds the limit as proposed in [20]. Especially in scenario 2 on the Y-intersection, the peak acceleration exceeds the proposed limit by 0.9 m s^{-2} . However, this peak occurs during deceleration and is necessary

to maintain a two second following distance. For most scenarios, the ego-vehicle is able to maintain decent time efficiency. However, in scenario 2 of the four-way intersection the TTI is 4.1 s, which means the ego-vehicle is more conservative than desired. These simulation results show that a model predictive controller is capable of behavior planning in a variety of urban scenarios, while constantly evaluating a trade-off between safety and comfort. Video footage of all simulated scenarios is available online and can be found through Appendix A.

Map	Scenario	Criterion	Value	
Roundabout	Scenario 1	Distance	6.2 m	
		TIV	6.2 s	
		Acceleration	-1.82 m s^{-2}	
		Jerk	2.3 m s^{-3}	
		TTI	1.6 s	
	Scenario 2	Distance	12.5 m	
		TIV	1.95 s	
		Acceleration	-1.6 m s^{-2}	
		Jerk	2.5 m s^{-3}	
	Scenario 3	Distance	12.6 m	
		TIV	2 s	
		Acceleration	-1.5 m s^{-2}	
		Jerk	2.4 m s^{-3}	
	Four-way Intersection	Scenario 1	Distance	19.9 m
			TIV	6.6 s
Acceleration			-2.3 m s^{-2}	
Jerk			2.6 m s^{-3}	
TTI			2.5 s	
Scenario 2		Distance	17.1 m	
		TIV	∞	
		Acceleration	-2.3 m s^{-2}	
		Jerk	2.8 m s^{-3}	
Y-Intersection		Scenario 1	Distance	15 m
			TIV	2.1 s
			Acceleration	-1.7 m s^{-2}
			Jerk	1.9 m s^{-3}
			TTI	1.6 s
		Scenario 2	Distance	31.3 m
	TIV		2 s	
	Acceleration		-2.4 m s^{-2}	
	Jerk		2.5 m s^{-3}	
			TTI	2.5 s

Table III: Summary of results of the simulations.

The simulations were performed on a platform with an Intel Core i7700k processor running at 4.2 GHz on a single core. The average KTT iteration of the model predictive controller has a calculation time of 2.68 ms with a minimum calculation time of 0.90 ms and a maximum of 3.11 ms. The entire process of situation analysis and behavior planning is able to run in real-time with a control input delay of less than 0.2 s.

V. DISCUSSION AND CONCLUSION

In this work the development of a novel longitudinal behavior planning method with maneuver prediction for driving in urban scenarios is presented. The behavior planning method makes use of a model predictive control scheme to optimize longitudinal acceleration of an intelligent vehicle in urban scenarios. The choice for a model predictive control-based behavior planner is based on the aim to develop a universal method that is applicable for a variety of urban scenarios, is capable of real-time performance and has a wide action set. It has been shown that by using a multi-layer situation analysis architecture, a universal model predictive controller is able to plan acceptable behavior for a variety of urban scenarios where traffic object trajectories are not known a priori. Within the situation analysis architecture, a Bayesian Network predicts the maneuvers of traffic objects on intersections and roundabouts. By combining these maneuver predictions with knowledge of the map, traffic object trajectories can be predicted. By approximating these trajectory predictions with a set of polynomials of a fixed form, the trajectories can be input to the universal model predictive controller.

Simulation results show that the behavior planning method correctly accounts for traffic object maneuvers, and is able to maintain an adequately safe distance to traffic objects. Comfort is judged based on longitudinal jerk, as well as acceleration and deceleration levels of the vehicle. The longitudinal jerk is shown to remain within acceptable limits, however the acceleration values are on the edge of acceptable limits for most scenarios. Real-time performance is maintained throughout the simulations. For future work, expansion of the behavior planning model to include lane change decision making and follow road laws is required for more complex multi-lane intersections. Moreover, for this work the assumption was made that the global coordinates, velocity and acceleration of all vehicles are observable. Because this assumption may not always be valid for real-life driving, additional research is needed to extend the behavior planning module for use with partial observability of the environment.

APPENDIX A SIMULATION VIDEO FOOTAGE

Video footage of all the simulated scenarios is made available through the TU Delft Repository at <https://repository.tudelft.nl/islandora/object/uuid:57f9a5f4-0608-42ca-b956-346afe5e4b7d?collection=> education. The video footage consists of the following files:

- Roundabout_S1.mp4: Top-down footage of roundabout scenario 1.
- Roundabout_S2.mp4: Top-down footage of roundabout scenario 2.
- Roundabout_S3.mp4: Top-down footage of roundabout scenario 3.
- Fourway_S1.mp4: Top-down footage of four-way intersection scenario 1.
- Fourway_S2.mp4: Top-down footage of four-way intersection scenario 2.

- YInt_S1.mp4: Top-down footage of Y-intersection scenario 1.
- YInt_S2.mp4: Top-down footage of Y-intersection scenario 2.

ACKNOWLEDGMENTS

I would like to thank my daily supervisor Mohsen Se-fati for the opportunity to do this research at the chair for Production Engineering of E-mobility Components (PEM) at RWTH Aachen University, and for the guidance on the global overview of this project. Furthermore I would like to thank the team at PEM for their support and feedback during this research project.

I would like to thank my supervisor Dr. Javier Alonso-Mora for his feedback on this work. Furthermore, I would like to thank Dr. ir. Riender Happee for his feedback and his help in arranging this exchange with RWTH Aachen University.

I would like to express my deepest gratitude to my family and friends for their love and support.

REFERENCES

- [1] World Health Organization, *Global status report on road safety 2015*. World Health Organization, 2015.
- [2] Kennisinstituut voor Mobiliteitsbeleid, *Mobiliteitsbeeld 2016*. Ministerie van Infrastructuur en Milieu, 2016.
- [3] S. Singh, *Critical reasons for crashes investigated in the national motor vehicle crash causation survey*. National Highway Traffic Safety Administration, 2015.
- [4] P. A. Ioannou and C.-C. Chien, "Autonomous intelligent cruise control," *IEEE Transactions on Vehicular Technology*, vol. 42, no. 4, pp. 657–672, 1993.
- [5] P. I. Labuhn and W. J. Chundrlik Jr, "Adaptive cruise control," Oct. 3 1995, uS Patent 5,454,442.
- [6] Tesla Motors, "Your autopilot has arrived," 2015.
- [7] AG Daimler, "Mercedes-benz intelligent drive tecday: Networked with all senses," *TecDay, Press Information*, vol. 19, 2012.
- [8] R. Matthaei and M. Maurer, "Autonomous driving—a top-down-approach," *at-Automatisierungstechnik*, vol. 63, no. 3, pp. 155–167, 2015.
- [9] C. Urmson, J. Anhalt, D. Bagnell, C. Baker, R. Bittner, M. Clark, J. Dolan, D. Duggins, T. Galatali, C. Geyer *et al.*, "Autonomous driving in urban environments: Boss and the urban challenge," *Journal of Field Robotics*, vol. 25, no. 8, pp. 425–466, 2008.
- [10] M. Bahram, A. Wolf, M. Aeberhard, and D. Wollherr, "A prediction-based reactive driving strategy for highly automated driving function on freeways," in *Intelligent Vehicles Symposium Proceedings, 2014 IEEE*. IEEE, 2014, pp. 400–406.
- [11] J. Nilsson and J. Sjöberg, "Strategic decision making for automated driving on two-lane, one way roads using model predictive control," in *Intelligent Vehicles Symposium (IV), 2013 IEEE*. IEEE, 2013, pp. 1253–1258.
- [12] D. Lenz, T. Kessler, and A. Knoll, "Tactical cooperative planning for autonomous highway driving using monte-carlo tree search," in *Intelligent Vehicles Symposium (IV), 2016 IEEE*. IEEE, 2016, pp. 447–453.
- [13] S. Brechtel, T. Gindele, and R. Dillmann, "Probabilistic decision-making under uncertainty for autonomous driving using continuous pomdps," in *Intelligent Transportation Systems (ITSC), 2014 IEEE 17th International Conference on*. IEEE, 2014, pp. 392–399.
- [14] J. Chandiramani, "Decision making under uncertainty for automated vehicles in urban situations," 2017.

- [15] J. Nilsson, M. Brännström, E. Coelingh, and J. Fredriksson, “Longitudinal and lateral control for automated lane change maneuvers,” in *American Control Conference (ACC), 2015*. IEEE, 2015, pp. 1399–1404.
- [16] J. Nilsson, M. Brännström, J. Fredriksson, and E. Coelingh, “Longitudinal and lateral control for automated yielding maneuvers,” *IEEE Transactions on Intelligent Transportation Systems*, vol. 17, no. 5, pp. 1404–1414, 2016.
- [17] B. Houska, H. Ferreau, and M. Diehl, “ACADO Toolkit – An Open Source Framework for Automatic Control and Dynamic Optimization,” *Optimal Control Applications and Methods*, vol. 32, no. 3, pp. 298–312, 2011.
- [18] S. Glaser, B. Vanholme, S. Mammar, D. Gruyer, and L. Nouveliere, “Maneuver-based trajectory planning for highly autonomous vehicles on real road with traffic and driver interaction,” *IEEE Transactions on Intelligent Transportation Systems*, vol. 11, no. 3, pp. 589–606, 2010.
- [19] Openbaar Ministerie. Bumperkleven. [Online]. Available: <https://www.om.nl/onderwerpen/verkeer/handhaving-verkeer/bumperkleven/>
- [20] L. L. Hoberock, “A survey of longitudinal acceleration comfort studies in ground transportation vehicles,” *Journal of Dynamic Systems, Measurement, and Control*, vol. 99, no. 2, pp. 76–84, 1977.
- [21] S. Lefèvre, D. Vasquez, and C. Laugier, “A survey on motion prediction and risk assessment for intelligent vehicles,” *Robomech Journal*, vol. 1, no. 1, p. 1, 2014.
- [22] M. Treiber, A. Hennecke, and D. Helbing, “Congested traffic states in empirical observations and microscopic simulations,” *Physical review E*, vol. 62, no. 2, p. 1805, 2000.
- [23] M. Schreier, V. Willert, and J. Adamy, “An integrated approach to maneuver-based trajectory prediction and criticality assessment in arbitrary road environments,” *IEEE Transactions on Intelligent Transportation Systems*, vol. 17, no. 10, pp. 2751–2766, 2016.
- [24] T. Gindele, S. Brechtel, and R. Dillmann, “Learning context sensitive behavior models from observations for predicting traffic situations,” in *Intelligent Transportation Systems-(ITSC), 2013 16th International IEEE Conference on*. IEEE, 2013, pp. 1764–1771.
- [25] A. Gray, Y. Gao, J. K. Hedrick, and F. Borrelli, “Robust predictive control for semi-autonomous vehicles with an uncertain driver model,” in *Intelligent Vehicles Symposium (IV), 2013 IEEE*. IEEE, 2013, pp. 208–213.
- [26] H. Ferreau, C. Kirches, A. Potschka, H. Bock, and M. Diehl, “qpOASES: A parametric active-set algorithm for quadratic programming,” *Mathematical Programming Computation*, vol. 6, no. 4, pp. 327–363, 2014.